NANO LETTERS

LETTER

pubs.acs.org/NanoLett

Magnetoelectric Coupling in Ordered Arrays of Multilayered Heteroepitaxial $BaTiO_3/CoFe_2O_4$ Nanodots

Xiaoli Lu,[*,†] Yunseok Kim,[*,†,§] Silvana Goetze,[†] Xiaoguang Li,[‡] Sining Dong,[‡] Peter Werner,[†] Marin Alexe,[†] and Dietrich Hesse[†]

[†]Max Planck Institute of Microstructure Physics, D-06120 Halle (Saale), Germany

[‡]Hefei National Laboratory for Physical Sciences at Microscale, Department of Physics, University of Science and Technology of China, Hefei 230026, China

Supporting Information

ABSTRACT: Fully epitaxial $BaTiO_3/CoFe_2O_4$ ferroelectric/ferromagnetic multilayered nanodot arrays, a new type of magnetoelectric (ME) nanocomposite with both horizontal and vertical orderings, were fabricated via a stencil-derived direct epitaxy technique. By reducing the clamping effect, ferroelectric domain modification and distinct magnetization change proportional to different interfacial area around the $BaTiO_3$ phase transition temperatures were found, which may pave the way to quantitative introducing of ME coupling at nanoscale and build high density multistate memory devices.

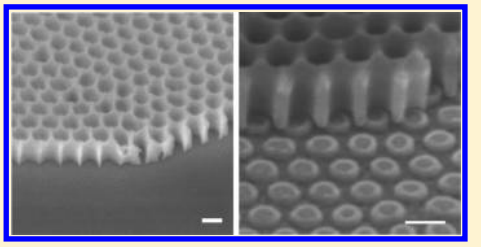

KEYWORDS: Multiferroic, nanodots, heterostructures, clamping effect, ME coupling

With the resurgence of interest in magnetoelectric (ME) multiferroics, the aspiration to build new types of memory devices with multistate data storage and heterogeneous read/write capability has fascinated researchers for decades.[1−4] Still, however, it is a big challenge to find proper materials with both multiferroic order and significant ME coupling at room temperature.[3] The fact that natural single-phase compounds rarely show strong coupling (especially at and above room temperature) brings about more and more interest in composite multiferroics. Stacking different components will not only combine their functionalities, namely ferroelectric (FE) and ferromagnetic (FM) properties, but also will provide efficient ways to tune the coupling through interfacial strain, exchange-bias, field effects, and so on.[4] Normally, ME composites can be labeled with the dimensionality of each component. For example, a 0−3 configuration means that there are two phases in the composite, one consisting of zero-dimension particulates, and the other is three-dimensional bulk.[5] As inspired by microelectronic industry, the research focus in ME composites has moved from bulk ceramics to film-on-substrate samples. Multilayered epitaxial thin films (2-2 configuration) were proposed first as a structure with strong ME coupling due to the high quality of crystallography and intimate coherent interface.[6] However, the clamping effect of the substrate onto the FE phase reduces the order of magnitude of the ME coupling coefficient up to a factor of 5 in thin films.[7] With the breakthrough in self-assembly vertical nanostructures (1-3 configuration) from immiscible perovskite and spinel systems, such as $CoFe_2O_4$ nanopillars embedded in a $BaTiO_3$ or $BiFeO_3$ matrix,[8−10] significant enhancement of ME coupling and electric-field induced magnetization switching[10] were found due to the large heteroepitaxial interface and reduced clamping effect. It makes ME nanocomposites promising candidates for a wide range of devices and has recently triggered intensive research activities. While the formation of 1-3 nanocomposites is highly dependent on the synthesis technique and the nature behind self-assembly behavior is not clear yet, the remaining open question is how to control the distribution ordering and expand the variety of 1-3 nanostructures.[11] Here, we propose a new structure: fully epitaxial multilayered nanodot arrays, noted as 0-0 composite as shown in Figure 1, which combines the advantages of 2-2 and 1-3 geometries. First, horizontal stacking like in an epitaxial multilayer or superlattice (2-2 type) can provide more flexibility for material design, composition control, and layer arrangement. Second, sizable ME coupling can be retained by reducing the clamping effect with much larger aspect ratio over conventional multilayer thin films.[12] Third, with the development in lithography techniques, distribution order of the composites will not be a problem. This new 0-0 heteroepitaxial nanostructure may help to obtain a better understanding of extrinsic ME coupling and build prototypes for high density multistate memory devices.

Generally, there are two ways to downscale the feature size of a material: (1) postpatterning, in which the sample is grown first and then selectively etched away chemically[13] or mechanically;[14] (2) in situ patterning, in which a stencil is used to confine the growth and transfer the pattern.[15] For multiferroic nanocomposites, the second way is more appropriate due to less contamination and less introduction of defects. This in situ patterning technique, also noted as stencil lithography, has recently developed very fast, as a simple and effective way to obtain nanowires, nanodots, and so forth.[16] Physical vapor deposition (PVD), such

Received: May 1, 2011
Revised: June 27, 2011
Published: July 12, 2011

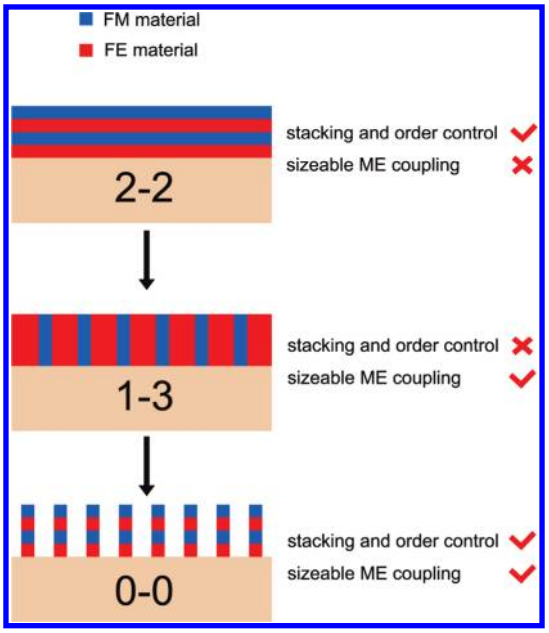

Figure 1. The evolution of ME composites with film-on-substrate geometry.

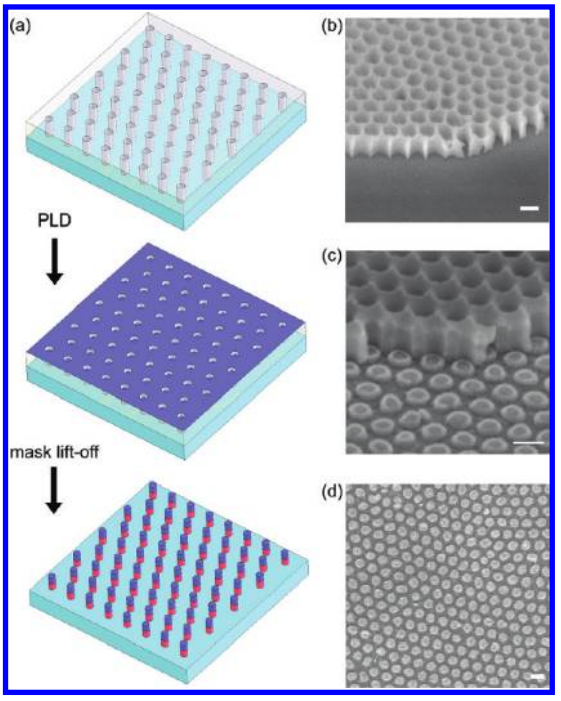

Figure 2. (a) Schematic illustration of AAO stencil-based nanofabrication. SEM images of (b) as-transferred AAO mask onto a STO substrate, (c) BTO nanodots with partially removed AAO after first layer deposition, and (d) BTO/CFO two-layered nanodot arrays. The sample stage was tilted 45° in (b) and (c) for a better view. The scale bars are 100 nm.

as pulsed laser deposition (PLD), molecular beam epitaxy (MBE), and so forth, is a widespread technique for well-controlled epitaxial growth of complex oxide films and heterostructures.[17] A combination of PVD and stencil lithography should allow the preparation of 0-0 composites. Technically, it requires the stencil to work as a shadow mask at elevated temperature (mostly higher than 400 °C). Then the stencil stability, surface diffusion, and blurring effect become remarkable,[15] which may hinder the pattern transfer and change the profile of the as-deposited structure. So it is not trivial to obtain epitaxial complex oxide nanodots, especially with a lateral size smaller than 100 nm. A successful growth relies on the right choice of the stencil and careful control of synthesis conditions. Recently, ultrathin anodic aluminum oxide (AAO) membranes were used as contact stencils to grow nanostructures by PLD.[18] They offer many advantages over silicon nitride membranes (another type of widely used stencil for high-temperature deposition) like low cost, more flexibility for thickness and feature size control, reduced blurring effect and surface diffusion with a direct attachment to the substrate, and so forth. Highly ordered $Pb(Zr_{0.2}Ti_{0.8})O_3$ (PZT)[18] and $CoFe_2O_4$[19] nanodot arrays with diameters from 40 to 350 nm were fabricated with this technique. However, due to the high aspect ratio (thickness over pore diameter) of the AAO mask, a low oxygen pressure (around 10^{-6} Torr) is normally needed in the stencil-based nanofabrication to maintain the direction of the plume (normal to the stencil for reducing shadowing effects) and enhance the energy of the impinging species,[18] which may induce a kinetic nonequilibrium growth and high density of oxygen vacancies.[20] The codeposited material on the stencil walls, on the other hand, may also disturb the growth and result in nanodots with curved surface.[21,22] More efforts are needed to improve the surface quality, so that multilayered epitaxial growth with AAO stencils still remains a challenge.

In this letter, fully epitaxial $BaTiO_3/CoFe_2O_4$ (BTO/CFO) multilayered nanodot arrays, that is, a 0-0 nanocomposite, were successfully fabricated by PLD at a relatively high oxygen pressure (around 10^{-2} Torr) through a modified AAO stencil mask. Abrupt, smooth, and coherent interfaces were obtained in these heterostructured nanodots, which is the basis for an effective strain mediated ME coupling. Quantitative magnetization changes around FE phase transition temperatures were found for the first time in nanodots with several layers, which may open a pathway to control the ME coupling at nanoscale and make an important step toward high density multistate memory devices.

The fabrication process is detailed in the Supporting Information, but schematically the flowchart is shown in Figure 2a. Briefly, the AAO mask with optimized aspect ratio was fabricated by a two-step anodization with oxalic acid. Thickness and pore diameter were carefully controlled by the second anodization time and a pore-widening process. After transferring the AAO membrane to the $SrTiO_3$ (STO) (001) substrate, isopropanol was dropped to the surface for improving the attachment. A typical scanning electron microscope (SEM) image of the as-obtained STO/AAO substrate is shown in Figure 2b. No gap was found between STO and the AAO membrane with thickness around 120 nm and pore diameters around 65 nm. In order to find the proper PLD parameters for a high-quality epitaxy with smooth surface, the deposition parameters were optimized by growing BTO and CFO films, respectively, on STO (001) with a fixed oxygen pressure around 10^{-2} Torr. Atomic force microscopy (AFM) images (Supporting Information Figure S1) and X-ray diffraction (XRD) patterns (Supporting Information Figure S2) confirmed the atomically flat epitaxial growth of BTO and CFO films at 650 °C. Because of the small aspect ratio and good attachment of the AAO mask, it is possible to deposit nanodots at the same conditions as the films, which guarantees a flat surface for the following epitaxy. As shown in Figure 2c,d, highly ordered nanodot arrays with flat surfaces and diameters around 65 nm were obtained, which indicates the successful pattern transfer during the growth. Since the AAO was fabricated through a self-assembly process, the periodic area is only μm^2 in

dx.doi.org/10.1021/nl201443h |*Nano Lett.* 2011, 11, 3202–3206

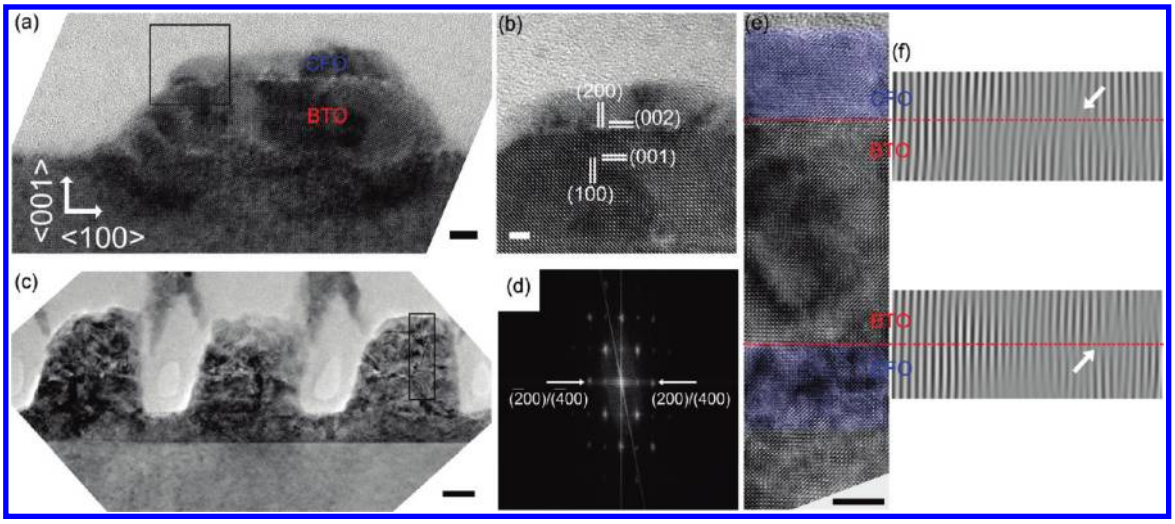

Figure 3. (a) TEM cross section view of a BTO/CFO nanodot in ⟨010⟩ projection. (b) HRTEM view of the framed area in (a). (c) TEM cross section view of BTO/CFO/BTO/CFO nanodots. The scale bar is 20 nm. (d) FFT pattern and (e) artificially colored HRTEM view of the framed area in (c). The scale bars of panels a, b, c, and e are 5, 2, 20, and 5 nm, respectively. (f) Magnified interfacial FFT-filtered images with the information only from (200)/(400) and ($\bar{2}$00)/($\bar{4}$00) planes. Dislocations are marked by arrows.

size. Long-range ordering in AAO is also achievable with an imprint technique (Supporting Information Figure S3). In this case, individually addressable BTO/CFO nanodot arrays with a density up to 176 G dots/inch^2 can be obtained, which is in analogy to ref 18.

Transmission electron microscopy (TEM) was used to investigate the quality of the as-deposited nanodots. As shown in Figure 3a, a randomly selected nanodot was sectioned by a standard focused-ion-beam technique and investigated in cross section. A clear two-layered structure with a stacking of BTO/CFO (10/5 nm) was found. The fairly flat surface is a proof of well-controlled deposition, which is in agreement with the SEM results. High-resolution TEM (HRTEM) analysis reveals the epitaxial growth of the nanodots, a sharp and clear interface was found between BTO and CFO (Figure 3b). The in-plane lattice constants calculated from HRTEM results ($a_{BTO} \sim 4.0$ Å, $a_{CFO} \sim 8.1$ Å) confirm the good epitaxy and indicate a compressive strain in the CFO layer (Supporting Information Figure S4).

With fixing the deposition parameters, the present approach provides a simple and reliable way to grow multilayered or even superlattice nanodots just by regularly switching to different targets during PLD. Thus the technique developed here is a universal strategy to control both the horizontal and vertical distribution order in a nanocomposite, which may help to combine different oxides at the nanoscale in a controllable manner to obtain new functionalities. Figure 3c shows well-defined nanodots with a BTO/CFO/BTO/CFO (20/10/20/10 nm) structure. Both the clear lattice images for each layer and fast Fourier transformation (FFT) patterns revealed a good epitaxy in these nanodots (Figure 3d,e). The FFT pattern is slightly deformed due to the rectangular shape of the selected area (as framed in Figure 3c). An inverse FFT image provides the filtered HRTEM information only from selected planes (Figure 3f), where the nice coherent stacking of BTO (200) and CFO (400) planes can be seen much more clearly. The low density of interfacial dislocations (as marked by the arrows in Figure 3f) is related to the high quality of these fully strained nanodots.

Piezoresponse force microcopy (PFM) was used to investigate the ferroelectric properties of as-prepared nanostructures at room temperature. For the PFM measurements, a $SrRuO_3$ film (thickness ~15 nm) was epitaxially grown on STO (001) as a bottom electrode. Single layer BTO nanodots (height ~20 nm) were first demonstrated as a reference (Figure 4a). Clear vertical piezoresponse of downward polarization was revealed by the vertical PFM (VPFM) images, while there was no lateral piezoresponse from lateral PFM (LPFM) images (not shown here). These results indicate a single c^--domain structure of the BTO nanodots and agree well with the (001) epitaxial configuration. Local piezoresponse was observed by hysteresis loop measurements at 25 kHz on individual BTO nanodot, which presents a soft ferroelectricity with small coercive voltage (~0.05 V). A horizontal shift, namely imprint, was also found in the hysteresis loop, which may be induced by an internal built-in field in the nanodot.[23] Different from the domain structures of BTO nanodots, as-prepared BTO/CFO (20/10 nm) nanodots show multidomain structures as shown in the VPFM image of Figure 4b. However, there was no lateral piezoresponse, which means that the domain structures of BTO/CFO nanodots are composed of c^+ and c^--domains without any *a*-domains. Hysteresis loops on individual BTO/CFO nanodots were measured with the same optimized parameters as for BTO nanodots, which allows properly comparing their properties and avoiding artifacts. Interestingly, no imprint was found in BTO/CFO nanodots, which means the additional layer of CFO on BTO may alter the depolarization field state in BTO nanodots. Associated with the multidomain structures, the CFO top layer certainly induced modifications onto the FE properties of BTO nanodots, which might be also relevant to the change of the depolarization field. However, we cannot exclude the change of interfacial strain via magnetostricion effect which can be a proof of successful strain coupling in the as-prepared nanocomposite. While the reasons for FE domain change (from c^- to c^-/c^+ mixture) and imprint are very complex, we cannot attribute these to ME coupling yet. Nevertheless, the present results from PFM measurements have clearly revealed that room temperature ferroelectricity is retained in the multilayered nanocomposites, and their polarization states can be easily switched by a small voltage.

Both the coherent heteroepitaxial interface and the observed FE domain modifications imply a promising ME coupling in the

dx.doi.org/10.1021/nl201443h |*Nano Lett.* 2011, 11, 3202–3206

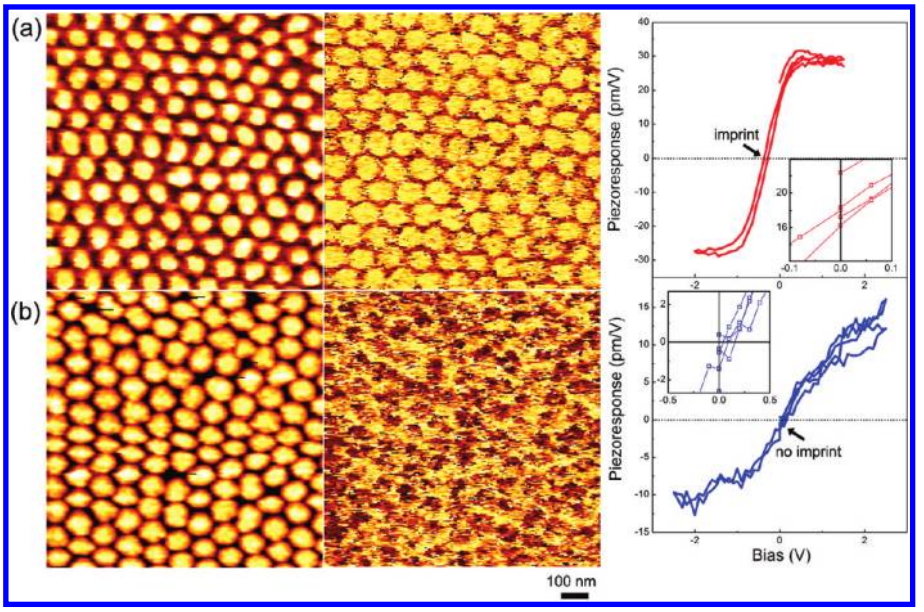

Figure 4. Topography, VPFM phase images and local piezoelectric hysteresis loops of (a) BTO nanodots and (b) BTO/CFO nanodots on STO/SRO substrate. The insets are enlarged loops around zero bias.

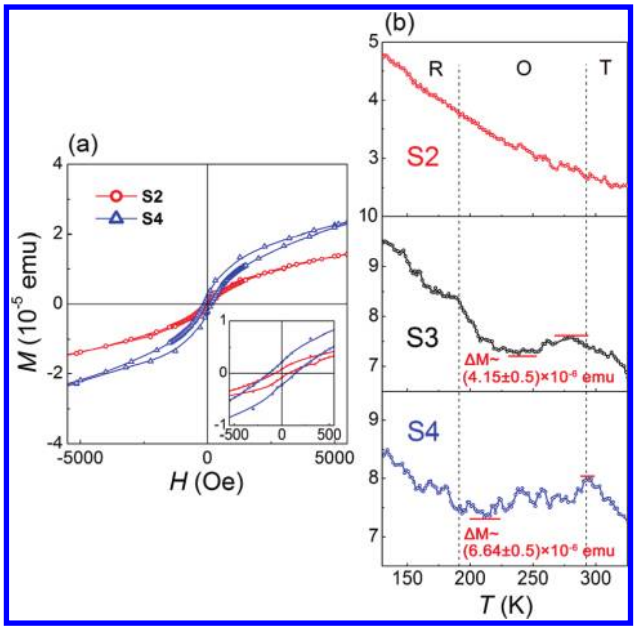

Figure 5. (a) Room-temperature magnetic hysteresis loops for as prepared two-layered (S2) and four-layered (S4) nanodots. The inset is the enlarged curve at the center. (b) Magnetization vs temperature curves for nanodots with different layers (S2, S3, and S4). The vertical dashed lines of (b) are guide to the eyes to indicate the structural phase transitions of BTO.

multilayered nanodots. Since the direct measurement is very difficult, the ME coupling was investigated by recording the magnetization change around BTO phase transition temperatures.[1] Hence, a superconducting quantum interference device (SQUID) was used to probe the magnetization of the as-prepared nanodots. Because of the cubiclike magnetic anisotropy in CFO nanodots,[21] all the data were collected with an in-plane field setup only. Figure 5a shows room temperature magnetization vs external field ($M-H$) curves of as-prepared different layered nanodots (S2: BTO/CFO, 20/10 nm and S4: BTO/CFO/BTO/CFO, 20/10/20/10 nm). After subtracting the signal from the substrate, clear hysteresis loops with similar coercive field (H_c) around 100 Oe indicate the room temperature ferromagnetism of the composite. As we know, with decreasing temperature bulk BTO experiences three phase transitions that are cubic-to-tetragonal (C to T, ~390 K), tetragonal-to-orthorhombic (T to O, ~290 K) and orthorhombic-to-rhombohedral (O to R, ~190 K).[24] The phase transition-induced crystallographic change or domain switching will alter the local strain in CFO and thus the magnetization.[25] As shown in Figure 5b, the magnetization was measured from 130 to 330 K in the zero-field cooling-down mode (external field H = 50 kOe). In the $M-T$ curve of S4, with the temperature decreasing magnetization increased first and showed a distinct kink around 290 K; then the slope of the $M-T$ curve changed, the magnetization decreased gradually to a minimum value and went back to normal around 190 K. Zheng et al. reported that for about 1−3 type CFO-BTO nanostructures, a similar drop in magnetization and a kink were also found around 390 K (BTO changes from C to T phase) and were attributed to ME coupling in the composite.[8] Since CFO is a negative magnetostriction material, the decrease of compression in CFO (when BTO changes from T to O or R phase) will induce a drop of the magnetization, so that the $M-T$ curve gets a kink and changes the slope. The total magnetization drop (ΔM) from 290 to 190 K can be calculated to $(6.64 \pm 0.5) \times 10^{-6}$ emu and, by normalizing the ΔM to the volume of the CFO nanodots, a sizable value was obtained around 76 emu/cm^3. (The detailed calculation is shown in the Supporting Information.) So far a clear ME coupling was found in S4 as shown by the kink in the $M-T$ curve and the ΔM, which indicates that the clamping effect was reduced and the coherent heteroexpitaxial interfaces effectively mediated the strain in this 0-0 nanocomposite. Unlike the abrupt and sharp magnetization changes, as found usually in magnetic films on BTO single crystals,[26] the strain-induced magnetization change in multilayered nanodots was distributed over a wide temperature range. This result is in agreement with a previous report about the broadened phase-transition behavior in nanosystems.[27] However, in the $M-T$ curve of S2, a typical FM behavior was found

dx.doi.org/10.1021/nl201443h |*Nano Lett.* 2011, 11, 3202–3206

without kink or ΔM. Unlike S4, there is only one BTO/CFO interface in S2. According to the report by Liu et al. for an about three-dimensional BTO−CFO heteroepitaxial nanocomposite,[28] the strain-induced ΔM is related to the interfacial area. In this context, another three-layered sample (S3: CFO/BTO/CFO, 10/20/10 nm, two interfaces) was prepared. A $\Delta M \sim (4.15 \pm 0.5) \times 10^{-6}$ emu and similar kink in the $M-T$ curve were found around the BTO phase transition. Most interesting is the observation that $\Delta M_{S4}/\Delta M_{S3} \sim 1.6$, which is close to the ideal interfacial area ratio of S4 and S3 (3/2 = 1.5). Then, in this way, ΔM in S2 can be around $(3.32 \pm 0.5) \times 10^{-6}$ emu instead of zero. Another unclear thing is the oscillations coming together with the strain-induced slope change in S3 and S4, which are not found in S2. Since the standard error of SQUID measurements is below 5×10^{-7} emu, which is far away from the order of magnitude level of samples' moment, the variations in the $M-T$ curves are reliable. The absence of ΔM in S2 and the oscillations all indicated that the dependence of magnetization-to-strain coupling in these new nanocomposites is more complicated than expected. Many factors like vortex structure, finite size effect, strain relaxation sideways, and so forth[29−31] may all play a role. More detailed experimental and theoretical investigations are required to obtain a better understanding, which may help to shed new light on strain-mediated multiferroics. Nevertheless, the results have already shown a sizable ME coupling[5] in this 0-0 nanocomposite, and to the best of our knowledge, the proportional change of magnetization with different interfacial area was revealed for the first time, which may open the way to precise quantification of ME coupling at the nanoscale.

In summary, a new type of ME composite was proposed, and well-ordered BTO/CFO multilayered nanodot arrays were fabricated with a modified AAO stencil technique, which can be a general approach to control both the horizontal and vertical distribution orders in functional oxide heterostructures at the nanoscale. Room-temperature multiferroic properties of the nanodots were proved by PFM and SQUID measurements. Because of the good heteroepitaxial interface and reduced clamping effect, elastic interaction can be effectively transferred resulting in a change of the FE and FM properties. This composite might make it feasible to control both the ME order (with different components) and degree of ME coupling (with different interfacial area) and can be an ideal prototype for a high density multistate memory device.

■ ASSOCIATED CONTENT

Supporting Information. Description of fabrication and measurements. This material is available free of charge via the Internet at http://pubs.acs.org.

■ AUTHOR INFORMATION

Corresponding Author

*E-mail: (X.L.) xllu@mpi-halle.de; (Y.K.) kimy4@ornl.gov.

Present Addresses

[§]The Center for Nanophase Materials Sciences, Oak Ridge National Laboratory, Oak Ridge, TN 37831.

■ ACKNOWLEDGMENT

The authors acknowledge German Science Foundation (DFG) for support via SFB 762 and the Alexander von Humboldt foundation (X.L. and Y.K.).

■ REFERENCES

(1) Eerenstein, W.; Mathur, N. D.; Scott, J. F. *Nature* **2006**, *442*, 759–765.
(2) Nan, C. W.; Bichurin, M. I.; Dong, S. X.; Viehland, D.; Srinivasan, G. *J. Appl. Phys.* **2008**, *103*, 031101−1–35.
(3) Spaldin, N. A.; Cheong, S. W.; Ramesh, R. *Phys. Today* **2010**, *63*, 38–43.
(4) Vaz, C. A. F.; Hoffman, J.; Anh, C. H.; Ramesh, R. *Adv. Mater.* **2010**, *22*, 2900–2918.
(5) Newnham, R. E.; Skinner, D. P.; Cross, L. E. *Mater. Res. Bull.* **1978**, *13*, 525–536.
(6) Avellaneda, M.; Harshe, G. *J. Intell. Mater. Syst. Struct.* **1994**, *5*, 501–513.
(7) Bichurin, M. I.; Petrov, V. M.; Srinivasan, G. *Phys. Rev. B: Condens. Matter Mater. Phys.* **2003**, *68*, 054402−1–13.
(8) Zheng, H.; Wang, J.; Lofland, S. E.; Ma, Z.; Mohaddes-Ardabili, L.; Zhao, T.; Salamanca-Riba, L.; Shinde, S. R.; Ogale, S. B.; Bai, F.; Viehland, D.; Jia, Y.; Schlom, D. G.; Wuttig, M.; Roytburd, A.; Ramesh, R. *Science* **2004**, *303*, 661–663.
(9) Zheng, H.; Wang, J.; Mohaddes-Ardabili, L.; Wuttig, M.; Salamanca-Riba, L.; Schlom, D. G.; Ramesh, R. *Appl. Phys. Lett.* **2004**, *85*, 2035–2037.
(10) Zavaliche, F.; Zheng, H.; Mohaddes-Ardabili, L.; Yang, S. Y.; Zhan, Q.; Shafer, P.; Reilly, E.; Chopdekar, R.; Jia, Y.; Wright, P.; Schlom, D. G.; Suzuki, Y.; Ramesh, R. *Nano Lett.* **2005**, *5*, 1793–1796.
(11) Yan, L.; Yang, Y. D.; Wang, Z. G.; Xing, Z. P.; Li, J. F.; Viehland, D. *J. Mater. Sci.* **2009**, *44*, 5080–5094.
(12) Nagarajan, V.; Roytburd, A.; Stanishevsky, A.; Prasertchoung, S.; Zhao, T.; Chen, L.; Melngailis, J.; Auciello, O.; Ramesh, R. *Nat. Mater.* **2003**, *2*, 43–47.
(13) Kustandi, T. S.; Loh, W. W.; Gao, H.; Low, H. Y. *ACS Nano* **2010**, *4*, 2561–2568.
(14) Ruzmetov, D.; Seo, Y.; Belenky, L. J.; Kim, D. M.; Ke, X. L.; Sun, H. P.; Chandrasekhar, V.; Eom, C. B.; Rzchowski, M. S.; Pan, X. Q. *Adv. Mater.* **2005**, *17*, 2869–2872.
(15) Vazquez-Mena, O.; Sannomiya, T.; Villanueva, L. G.; Voros, J.; Brugger, J. *ACS Nano* **2011**, *5*, 844–853.
(16) Gates, B. D.; Xu, Q. B.; Stewart, M.; Ryan, D.; Willson, C. G.; Whitesides, G. M. *Chem. Rev.* **2005**, *105*, 1171–1196.
(17) Chambers, S. A. *Adv. Mater.* **2010**, *22*, 219–248.
(18) Lee, W.; Han, H.; Lotnyk, A.; Schubert, M. A.; Senz, S.; Alexe, M.; Hesse, D.; Baik, S.; Gosele, U. *Nat. Nanotechnol.* **2008**, *3*, 402–407.
(19) Gao, X. S.; Liu, L. F.; Birajdar, B.; Ziese, M.; Lee, W.; Alexe, M.; Hesse, D. *Adv. Funct. Mater.* **2009**, *19*, 3450–3455.
(20) Evans, J. W.; Thiel, P. A.; Bartelt, M. C. *Surf. Sci. Rep.* **2006**, *61*, 1–128.
(21) Gao, X. S.; Rodriguez, B. J.; Liu, L. F.; Birajdar, B.; Pantel, D.; Ziese, M.; Alexe, M.; Hesse, D. *ACS Nano* **2010**, *4*, 1099–1107.
(22) Han, H.; Park, Y. J.; Baik, S.; Lee, W.; Alexe, M.; Hesse, D.; Gosele, U. *J. Appl. Phys.* **2010**, *108*, 044102−1–6.
(23) Ma, W. H.; Hesse, D. *Appl. Phys. Lett.* **2004**, *84*, 2871–2873.
(24) Polisetty, S.; Echtenkamp, W.; Jones, K.; He, X.; Sahoo, S.; Binek, C. *Phys. Rev. B: Condens. Matter Mater. Phys.* **2010**, *82*, 134419−1–7.
(25) Eerenstein, W.; Wiora, M.; Prieto, J. L.; Scott, J. F.; Mathur, N. D. *Nat. Mater.* **2007**, *6*, 348–351.
(26) Lee, M. K.; Nath, T. K.; Eom, C. B.; Smoak, M. C.; Tsui, F. *Appl. Phys. Lett.* **2000**, *77*, 3547–3549.
(27) Smith, M. B.; Page, K.; Siegrist, T.; Redmond, P. L.; Walter, E. C.; Seshadri, R.; Brus, L. E.; Steigerwald, M. L. *J. Am. Chem. Soc.* **2008**, *130*, 6955–6963.
(28) Liu, B.; Sun, T.; He, J. Q.; Dravid, V. P. *ACS Nano* **2010**, *4*, 6836–6842.
(29) Raabe, J.; Pulwey, R.; Sattler, R.; Schweinbock, T.; Zweck, J.; Weiss, D. *J. Appl. Phys.* **2000**, *88*, 4437–4439.
(30) Leite, V. S.; Godoy, M.; Figueiredo, W. *Phys. Rev. B: Condens. Matter Mater. Phys.* **2005**, *71*, 094427−1–7.
(31) Nan, C. W.; Liu, G.; Lin, Y. H.; Chen, H. D. *Phys. Rev. Lett.* **2005**, *94*, 197203−1–4.